IEEE Access
Multidisciplinary | Rapid Review | Open Access Journal

Received March 20, 2018, accepted April 12, 2018, date of publication April 19, 2018, date of current version June 5, 2018.

Digital Object Identifier 10.1109/ACCESS.2018.2828160

Kirchhoff Beam Migration Based on Compressive Sensing

HUI SUN[1,2], ZHIHOU ZHANG[1], GUANGMIN HU[2], FANCHANG MENG[3], CHENG GAO[4], MINGCHEN LIU[5], JING TANG[6], YAOJUN WANG[2], AND FEILONG YANG[7]

[1]MOE Key Laboratory of High-Speed Railway Engineering, Southwest Jiaotong University, Chengdu 610031, China
[2]School of Resources and Environment, University of Electronic Science and Technology of China, Chengdu 611731, China
[3]Institute of Geology and Geophysics, Chinese Academy of Sciences, Beijing 100029, China
[4]School of Mines, Inner Mongolia University of Technology, Huhhot 010051, China
[5]College for Geoexploration Science Technology, Jilin University, Changchun 130026, China
[6]School of Geoscience and Technology, Southwest Petroleum University, Chengdu 610500, China
[7]School of Earth Sciences and Engineering, Xi'an Shiyou University, Xi'an 710065, China

Corresponding author: Zhihou Zhang (logicprimer@163.com)

This work was supported in part by the Natural Science Foundation of China under Grant U1562218, Grant 41674140, Grant 41604107, Grant 41672295, and Grant 41702304, in part by the Fundamental Research Funds for the Central Universities, in part by the Science Research Project of the Inner Mongolia University of Technology under Grant ZD201622, in part by the Science Research Project of the Institutions of Higher Learning in Inner Mongolia under Grant NJZZ18079, and in part by the China Geological Survey Project under Grant 121201011000150013-05.

ABSTRACT Kirchhoff beam migration (KBM) is a seismic-signal-based imaging method that considers both computational efficiency and computational precision. This method requires the decomposition of the seismic records, at each center-window, to plane waves in different directions. KBM achieves this step via the conventional linear Radon transform (LRT), which has obvious drawbacks. First, many noises and spatial aliasing exist in the transform result; and second, the resolution of the result does not meet a pre-defined threshold. These drawbacks could affect the imaging ability of KBM. To solve these problems, this paper introduced a high-resolution LRT method based on compressive sensing to KBM to improve the quality of the obtained plane waves and imaging results. This paper verifies the seismic-signal imaging method via multiple numerical models.

INDEX TERMS Signal processing, compressive sensing (CS), seismic imaging method, local plane wave decomposition, prestack depth migration.

I. INTRODUCTION

Prestack depth migration is an important imaging method of seismic signal processing, which has been widely applied in oil exploration and earthquake research [1]–[5]. It can generally be divided into two classed, ray-based methods [6], [7] and finite-difference methods [8]–[10]. Beam migration is a kind of ray-based method, that can calculate multi-arrivals and boasts a high calculation accuracy and efficiency. Gaussian beam migration (GBM), first described by Hill in 1990, laid the theoretical foundation for beam migration [11]. The initial form of GBM is a poststack migration method. Sun *et al.* combined the beam implementation with Kirchhoff prestack depth migration to improve the imaging method's computational efficiency and proved it was efficient in the 3D case [12]. Hill developed Gaussian beam migration into a prestack migration method that could operate on common-offset seismic data sets [13]. In this method, the steepest descent method was adopted to improve the calculating efficiency, which was also employed by Gao *et al.* in 2015 [14]. Prestack Gaussian beam migration was later used for processing of common-source data sets [15]–[17]. Sherwood *et al.* [18], [19] presented another kind of beam imaging method. Shi *et al.* [20] proposed a time-domain depth migration method by summing the delta packets. This method images the complex subsurface structures by computing a point-to-point mapping and was successfully applied to examples from around the world. In addition to being used in conventional surface conditions, Gaussian beam migration is also used for seismic data processing under complex surface conditions [21]–[23]. Based on the true-amplitude migration theory put forward by Bleistein and Gray [24] and Zhang *et al.* [25], attempts were made by Gray and Bleistein [26] to obtain the amplitude information via GBM. Two versions of true-amplitude GBM

were developed, which were respectively based on a cross-correlation imaging condition and deconvolution imaging condition. Popov *et al.* [27] presented the GBM summation method, which strictly follows the Kirchhoff migration principles. Compared to Hill's GBM algorithm, this method has a higher accuracy but lower-computational efficiency, so it is usually used in oriented regional imaging. A multi-arrival Kirchhoff beam migration method was introduced by Liu and Palacharla; it is designed to focus on obtaining kinematic accuracy and computianal efficiency [28]. Only Kinetic Radial Tracing (KRT) equations are solved using this method. Two years later, KBM was developed from a common-offset algorithm to a common-source algorithm [29]. Beam migration methods are also used for multi-wave velocity analysis [30] and for compensating for the attenuation in multicomponent seismic data [31]. Sun *et al.* [32], [33] applied beam migration methods to migrate the complex deep-water model. After that, they combined the fast marching method (FMM) and wavefront construction method (WFC) to obtain a high-accuracy traveltime computing method [34], [35]. Li *et al.* [36] developed the preconditioned prestack plane wave least-squares reverse-time migration.

Beam migration is required to decompose seismic data into plane waves [37]–[39]. This step significantly affects the efficiency and imaging accuracy of the migration algorithm. Many scholars focus on this research. Hu and Stoffa (2009) [40] developed a slow-driven GBM for low-fold seismic data. Compared to conventional GBM, the method redefines the weighting function in the imaging formula to enhance the contribution that effective signals provide to the final imaging result. Yang *et al.* [41] also studied the weighting function, that further verified the validity of this method for real seismic data. Wu *et al.* [42] introduced a high-resolution LRT to the beam migration process to improve the accuracy of the imaging result. In the same year, Wu *et al.* [43] develop the 3D migration method. Wang *et al.* [44], [45] studied the plane wave decomposition-based compressive sensing (CS) method and introduced the characteristic-wave imaging method. Liu *et al.* [46] employed the same method for anisotropic seismic data processing. Huang *et al.* [47] created a modeling method for heterogeneous media by summing the Gaussian beam based Green's function.

The Kirchhoff beam migration method is further studied in this paper. A high-resolution LRT method, based on CS, is employed to improve the calculation accuracy of plane wave data and the quality of the final imaging result. The imaging ability of the modified KBM based on CS (CS-KBM) is verified by several numerical models, including the deep-water model, Marmousi model and 2D SEG/EAGE salt model.

II. METHODS

The key steps of KBM include:

1) Imaging principle of KBM,
2) beam geometry,
3) traveltime calculation,
4) amplitude calculation,
5) local plane wave decomposition.

The algorithm steps are described in detail in the next few sections.

A. KIRCHHOFF BEAM MIGRATION

KBM is a seismic imaging method focusing on rapid imaging of underground structures. The imaging principle is delineated by setting the common-source KBM as an example.

When the position of the source $\mathrm{x}_s(x_s, z_s)$ is determined, the imaging result the of subsurface node $\mathrm{x}(x, z)$ can be expressed as [29]:

$$I_s(\mathrm{x}) = \sum_L \int dp_s \int dp_{bc} A \cdot D_s \quad (L, p = p', \tau = \tau') \quad (1)$$

where $I_s(\mathrm{x})$ refers to the imaging result of point $\mathrm{x}(x, z)$; L is the series of window centers; p_s refers to the slowness of rays emitted from the source; p_{bc} refers to the slowness of rays emitted from the window center; A is the weight function; and $D_s(L, p, \tau)$ is the plane wave data. From (1), the migration results are obtained by adding up the results from every ray pair. However, this process doesn't apply imaging to all the grid nodes. The computational area shall be selected to guarantee the migration method's calculating efficiency. As shown in Fig. 1, the coverage area of the beam emitted from the source is labeled as Bs; the coverage area of beam emitted from the beam center is labeled as Bg; the deep shadow area A, the overlapping Bs and Bg areas, are selected to be imaged.

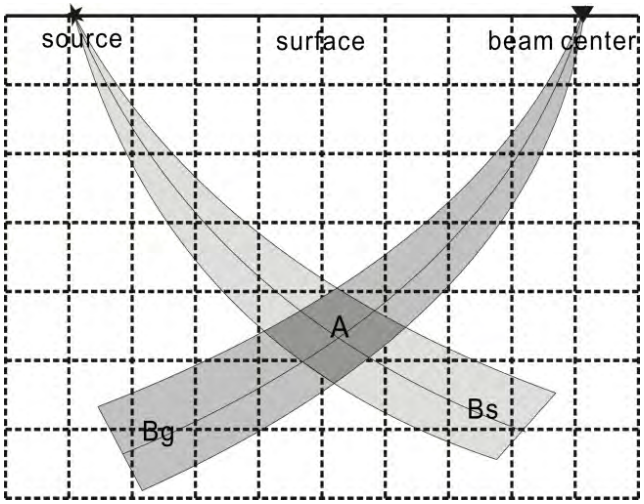

FIGURE 1. The sketch map of choosing the imaging points, Bg and Bs respectively represent ray beam from source and beam center.

The corresponding imaging conditions of (1) are:

$$\tau' = t_s + t_g \quad (2)$$

$$p' = p_{bc} \quad (3)$$

where, p_{bc} is the slowness of the ray emitted from the beam center; t_s refers to the traveltime from source to the imaging node; t_g refers to the traveltime from beam center to the imaging node;

B. BEAM GEOMETRY

Only kinematic ray tracing equations are solved by KBM to improve computational efficiency. We cannot obtain the dynamic parameters, which are essential for a Gaussian beam. In KBM, the beam width is calculated at every discrete point along the central ray.

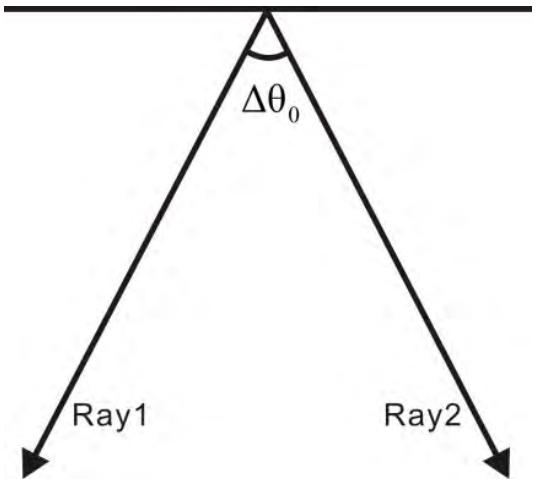

FIGURE 2. The sketch map for calculating the optimal beam width.

As is shown in Fig.2, the distance between two adjacent rays at **x** is given by

$$d = \Delta\theta_0 \left\| \frac{\partial \mathbf{x}}{\partial \theta_0} \right\| \tag{4}$$

where, $\Delta\theta_0$ is the angle interval between the adjacent rays. The beam width at **x** is

$$w_o = 2d = 2\Delta\theta_0 \left\| \frac{\partial \mathbf{x}}{\partial \theta_0} \right\| \tag{5}$$

The constant coefficient 2 is added to ensure the overlap area of the two adjacent beams is enough. When the velocity is only related to depth, we have

$$\frac{\partial x}{\partial \theta_0} = \frac{\cos\theta_0}{V_0}\sigma \tag{6}$$

$$\frac{\partial z}{\partial \theta_0} \approx -\frac{\sin\theta_0}{V_0}\sigma \tag{7}$$

where, V_0 is the velocity value at the ray launch position; σ is the integral of velocity along the ray path and can be expressed as $\int v\mathrm{d}s$. The norm of $\partial\mathbf{x}/\partial\theta_0$ can be expressed as

$$\left\| \frac{\partial \mathbf{x}}{\partial \theta_0} \right\| = \sqrt{\left(\frac{\partial x}{\partial \theta_0}\right)^2 + \left(\frac{\partial z}{\partial \theta_0}\right)^2} \approx \frac{\sigma}{V_0} \tag{8}$$

A simplified formula for (5) is

$$w_o = 2\Delta\theta_0 \frac{\sigma}{V_0} \tag{9}$$

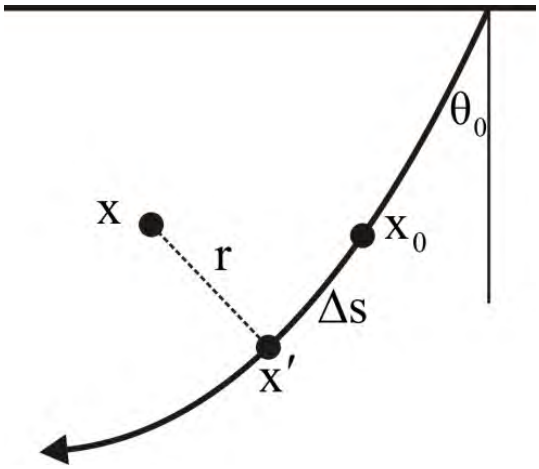

FIGURE 3. The sketch map of the traveltime computation.

C. TRAVELTIME CALCULATION

Traveltime is important for prestack depth migration, which can affect the focusing of the migration energy. In beam migration methods, traveltime is obtained by extrapolating the information of nodes via central rays. As shown in Fig. 3, x is the node within the beam, x_0 is the discrete point along the central ray, which is nearest to x, x' is the projection of x along the central ray, r is the distance from x to x' and Δs is the distance from x' to x_0. The traveltime of x can be expressed by:

$$t(\mathrm{x}) = t(\mathrm{x}_0) + \frac{\Delta s}{V} - \frac{(\Delta s)^2}{2V^2}\frac{\partial V}{\partial s} + \frac{1}{2}r^2 m_r \tag{10}$$

where V is the velocity and m_r is [48]

$$m_r = \mathrm{Re}\left(\frac{P}{Q}\right) \tag{11}$$

where P and Q are dynamical parameters, that cannot be obtained in KBM. If the velocity is smooth enough, then

$$Q = Q_0 + P_0\sigma \tag{12}$$

P_0 and Q_0 (Hill, 1990) are

$$Q_0 = \cos^2(\theta_0)\frac{V_{avg}^2}{2\pi V_0 f_{\min}} \tag{13}$$

$$P_0 = \frac{i}{V_0} \tag{14}$$

where, V_{avg} is the average value of the velocity field, $f_{\min}$ is the reference frequency and the initial beam width is defined as $\cos(\theta_0)V_{avg}/2\pi f_{\min}$. The term m_r can be further expressed by

$$\begin{aligned} m_r &= \mathrm{Re}\left(\frac{P_0}{Q_0 + P_0\sigma}\right) = \mathrm{Re}\left(\frac{i}{V_0 Q_0 + i\sigma}\right) \\ &= \mathrm{Re}\left(\frac{i}{\sigma_0 + i\sigma}\right) = \frac{\sigma}{\sigma^2 + \sigma_0^2} \end{aligned} \tag{15}$$

and

$$\sigma_0 = \cos^2(\theta_0)\frac{V_{avg}^2}{2\pi f_{\min}} \tag{16}$$

D. AMPLITUDE CALCULATION

Dynamical parameters cannot be obtained during the implementation of KBM. The accurate amplitude information is not needed in KBM. Therefore, amplitude calculation method of KBM is different from that of GBM. The calculation method is rough estimate, which mainly based on the principle: the closer to the central ray, the larger the weight function. There are two reasons for choosing the principle. One is that the closer the central ray, the stronger the energy is. The other reason is the grid points' traveltime is calculated by Taylor expansion, which is affected by the distance. The smaller the distance is, the more accurate the traveltime is.

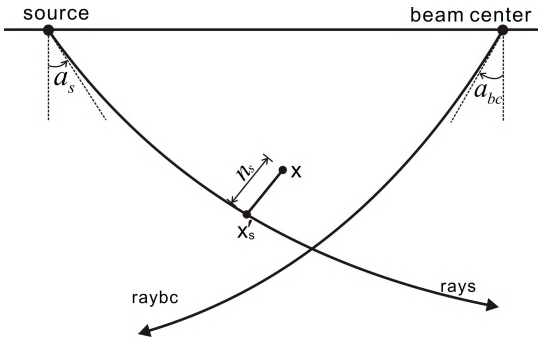

FIGURE 4. Schematic diagram of amplitude calculation.

As shown in Fig. 4, rays and raybc are emitted from the source and beam center, respectively. The emitted angle from the source is a_s; the emitted angle from the beam center is a_{bc}; x is the target point; x'_s is the target point's projection on rays; the distance between x and x'_s is n_s; the beam width at x'_s is w_s; the corresponding distance and beam width of raybc are n_{bc} and w_{bc}, respectively. The weight function of the target point can be expressed by

$$A = \cos^2\left[\frac{\pi}{4}\left(n_s^2 w_s^{-2} + n_{bc}^2 w_{bc}^{-2}\right)\right]\cos\left[0.5*(a_s - a_{bc})\right] \tag{17}$$

The extra term $\cos[0.5*(a_s - a_{bc})]$ is added to reduce the post-critical energy of the beam migration method.

E. LOCAL PLANE WAVE DECOMPOSITION

To image the subsurface nodes, decomposing the seismic records into plane waves is required. KBM employ LRT to finish this task [28], [29].

If the frequency seismic record is $\boldsymbol{D}(\omega)$, the frequency plane wave result is $\boldsymbol{P}(\omega)$. Their expressions are

$$\boldsymbol{D}(\omega) = [x_1(\omega), x_2(\omega), \cdots, x_{nx}(\omega)]^{\mathrm{T}} \tag{18}$$

$$\boldsymbol{P}(\omega) = [p_1(\omega), p_2(\omega), \cdots, p_{np}(\omega)]^{\mathrm{T}} \tag{19}$$

where, nx refers to the trace number of seismic records; np refers to the number of slowness samples; $x_1(\omega) \sim x_{nx}(\omega)$ refers to the received seismic signals; $p_1(\omega) \sim p_{nx}(\omega)$ is the plane wave data; Their relationship can be expressed by

$$\boldsymbol{D}(\omega) = \boldsymbol{L}(\omega)\boldsymbol{P}(\omega) \tag{20}$$

where, $\boldsymbol{L}(\omega)$ is

$$\boldsymbol{L}(\omega) = \begin{bmatrix} e^{iwp_1(x_1-x_L)} & e^{iwp_2(x_1-x_L)} & \cdots & e^{iwp_{np}(x_1-x_L)} \\ e^{iwp_1(x_2-x_L)} & e^{iwp_2(x_2-x_L)} & \cdots & e^{iwp_{np}(x_2-x_L)} \\ \cdots & \cdots & & \cdots \\ e^{iwp_1(x_{nx}-x_L)} & e^{iwp_2(x_{nx}-x_L)} & \cdots & e^{iwp_{np}(x_{nx}-x_L)} \end{bmatrix} \tag{21}$$

In (20) and (21), x_L is the location of the selected window. $\boldsymbol{L}(\omega)$ is a matrix with an $nx \times np$ surface area. Because this formulation is not represented by a square-matrix, its inverse matrix can be expressed by

$$\boldsymbol{L}^{-1}(\omega) = [\boldsymbol{L}^{\boldsymbol{H}}(\omega)\boldsymbol{L}(\omega)]^{-1}\boldsymbol{L}^{\boldsymbol{H}}(\omega) \tag{22}$$

where $\boldsymbol{L}^{\boldsymbol{H}}(\omega)$ is the conjugate transpose of $\boldsymbol{L}(\omega)$. To guarantee the stability of the solution, it is necessary to add the damping factor $\boldsymbol{I}(\omega)$ to the calculation. Thus, the expression of $\boldsymbol{P}(\omega)$ is

$$\boldsymbol{P}(\omega) = [\boldsymbol{L}^{\boldsymbol{H}}(\omega)\boldsymbol{L}(\omega) + \beta\boldsymbol{I}(\omega)]^{-1}\boldsymbol{L}^{\boldsymbol{H}}(\omega)\boldsymbol{D}(\omega) \tag{23}$$

These formulas are the calculating steps of conventional LRT.

CS-LRT decomposes seismic data into plane waves from the perspective of inversion. Thus, the minimized target function can be characterized by

$$\boldsymbol{J} = \|\boldsymbol{D}(\omega) - \boldsymbol{L}(\omega)\boldsymbol{P}(\omega)\|^2 + \|\boldsymbol{W}_{\boldsymbol{P}}(\omega)\boldsymbol{P}(\omega)\|^2 \tag{24}$$

where, $\boldsymbol{W}_{\boldsymbol{P}}(\omega)$ is a space-weighted matrix. After taking the derivative of $\boldsymbol{P}(\omega)$ and setting it to 0. Then, the following solution is obtained

$$\boldsymbol{P}(\omega) = [\boldsymbol{L}^{\boldsymbol{H}}(\omega)\boldsymbol{L}(\omega) + \boldsymbol{W}_{\boldsymbol{P}}^{-1}(\omega)]^{-1}\boldsymbol{L}^{\boldsymbol{H}}(\omega)\boldsymbol{D}(\omega) \tag{25}$$

The $\boldsymbol{L}_0$ norm is introduced to express the sparsity of the plane wave results. The plane wave decomposition can be expressed as

$$\begin{aligned} &\min\ \|\boldsymbol{P}(\omega)\|_0^0, \\ &S.T.\ \|\boldsymbol{D}(\omega) - \boldsymbol{L}(\omega)\boldsymbol{P}(\omega)\|_2^2 < \varepsilon \end{aligned} \tag{26}$$

where, ε refers to the noise of the target data. Then, we can obtain high-quality plane wave data by employing CS-LRT.

Fig. 5 (a) shows the synthesized data of multiple plane waves. Fig. 5 (b) shows the result of applying conventional LRT to the data in Fig. 5 (a). And Fig. 5 (c) shows the result of applying CS-LRT to the data in Fig. 5 (a). The results obtained with conventional LRT demonstrate space aliasing and truncation effects. In the $\tau - p$ domain, the data appears to have scissor-like divergence. CS-LRT has improved truncation effect suppression in the $\tau - p$ domain, where the divergent energies are convergent. So, CS-LRT could obtain plane wave data with higher resolution and better quality, which is essential for beam migration algorithms.

The common-source KBM flow char is shown in Fig. 6.

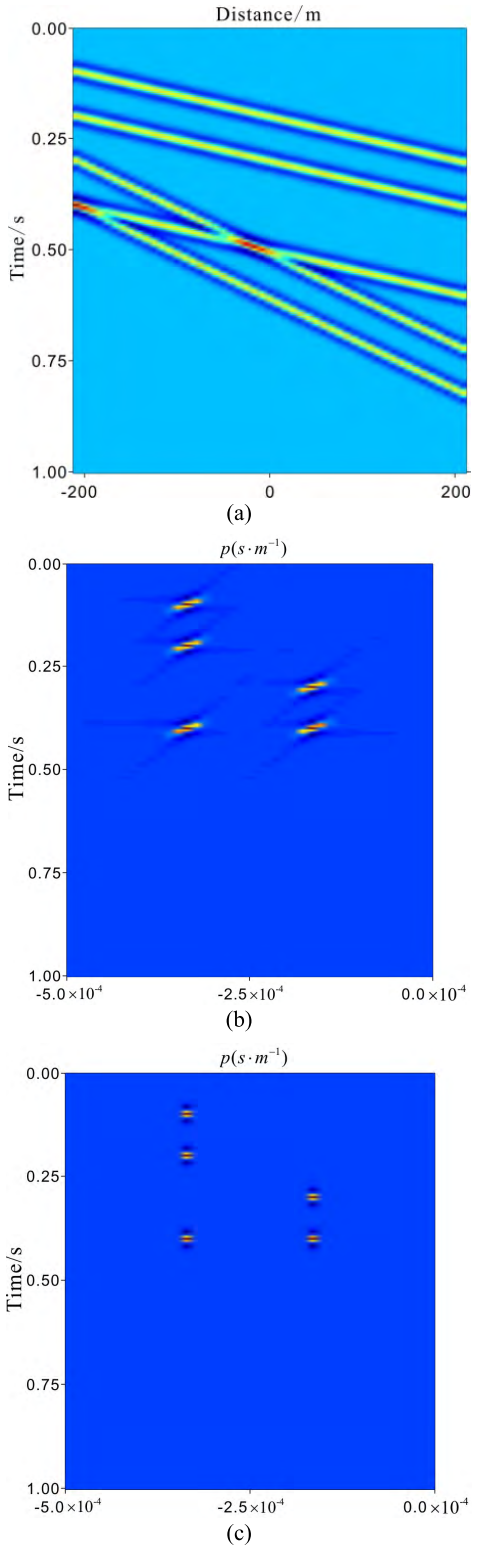

FIGURE 5. Decomposition results of synthesized data using different methods. (a) synthesized data of multiple plane waves; (b) result using the conventional LRT; (c) result using CS-LRT.

III. EXPERIMENTS AND ANALYSIS

This part employs the deep water model, the Marmousi model and the 2D SEG/EAGE salt model to test the imaging ability of CS-KBM.

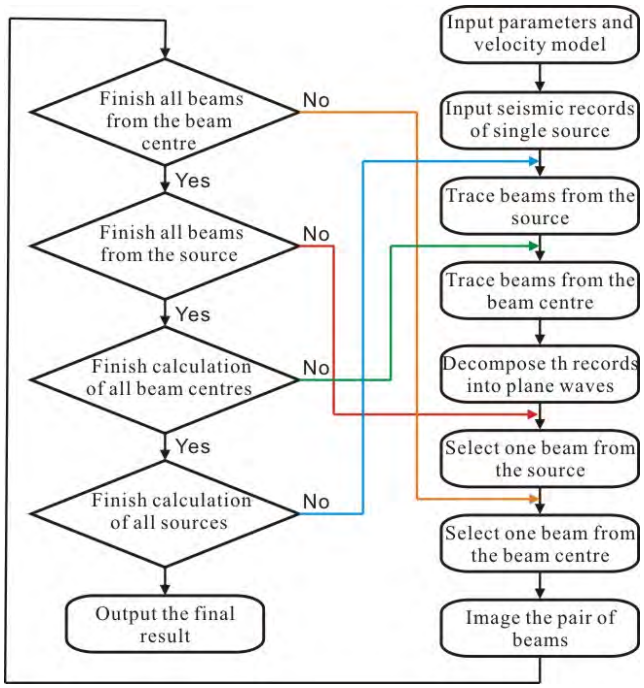

FIGURE 6. The flow chart of common-source KBM.

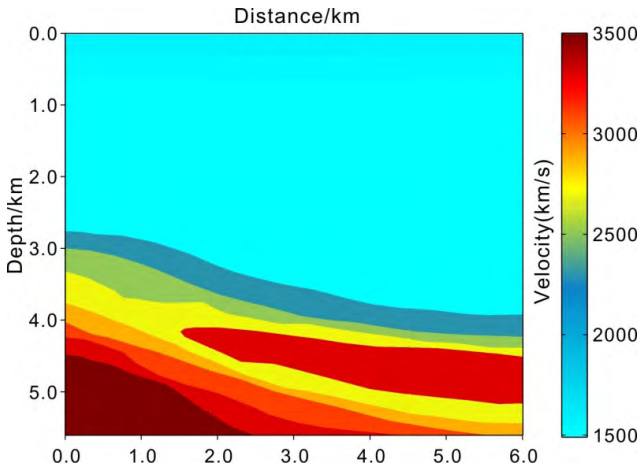

FIGURE 7. Deep water velocity model.

A. MIGRATION IMAGING OF DEEP WATER MODEL

Fig. 7 is the velocity of the deep water model, with a model size of 1501×1401; the grid spacing is 4 m both in the vertical and horizontal directions; the velocity of layers is 2500 m/s, 2700 m/s, 2900 m/s, 3000 m/s, 3100 m/s, 3300 m/s and 3500 m/s from up to down, respectively; the velocity of embedded body is 3300 m/s. The seismic data sets of the deep water model contain 59 shots; each shot has 480 traces with a trace interval of 20 m; each trace has 2000 samples with a sample rate of 3 ms.

Fig. 8 reveals the imaging results of the deep water model using different migration methods. Fig. 8 (a) shows the results of applying the KBM method; Fig. 8 (b) shows the results of applying the CS-KBM method; Fig. 8 (c) shows the partial

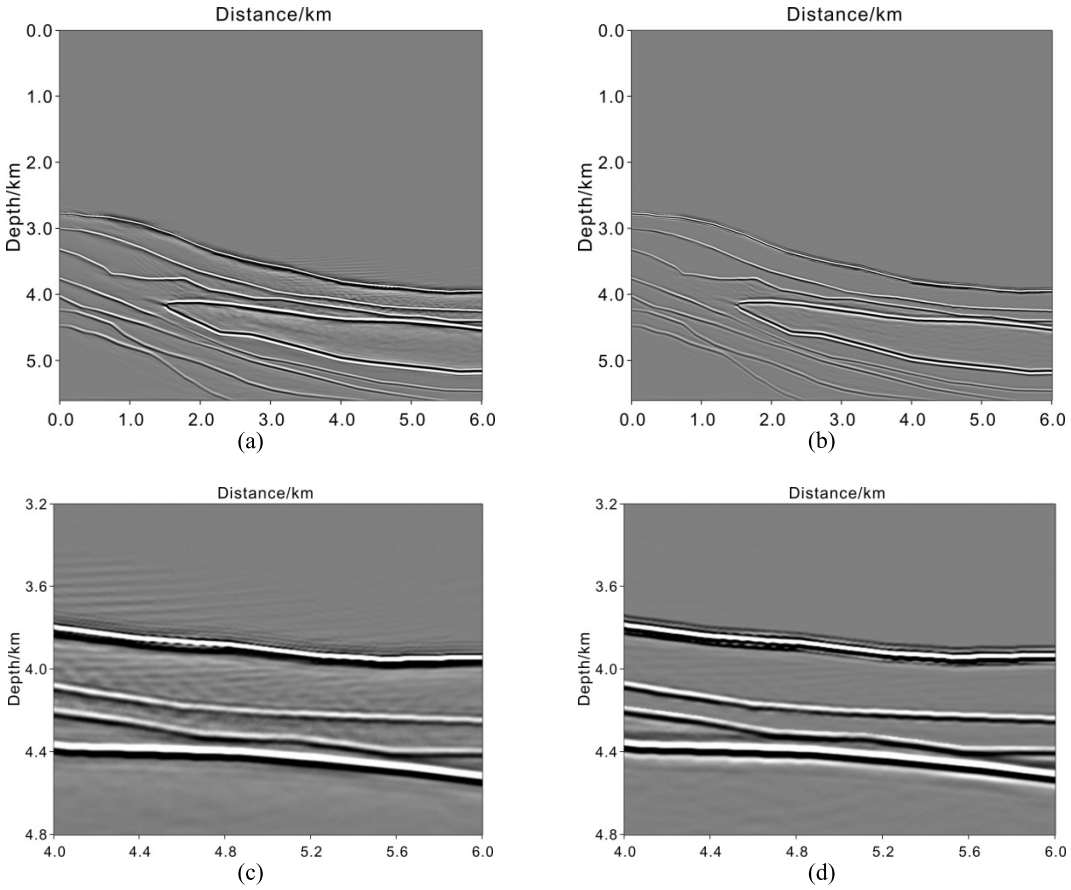

FIGURE 8. Comparison diagrams of imaging results for deep water model. (a) imaging result using the KBM method; (b) imaging result of using the CS-KBM method;(c) partial enlarged detail of imaging result of KBM; (d) partial enlarged detail of imaging result of CS-KBM.

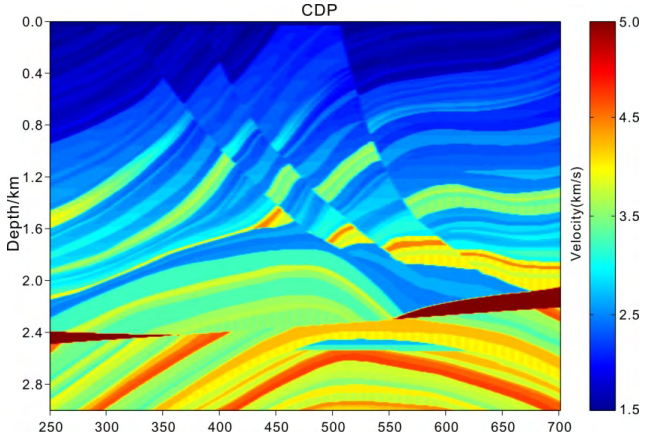

FIGURE 9. Marmousi velocity model.

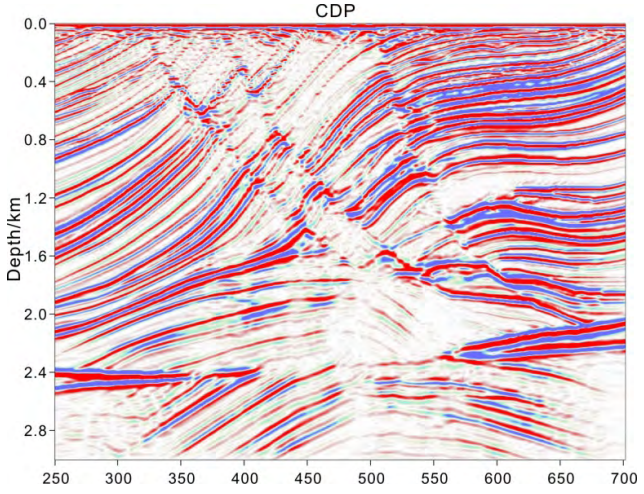

FIGURE 10. Marmousi velocity model.

enlarged detail of Fig. 8 (a); Fig. 8 (d) shows the partial enlarged detail of Fig. 8 (b). For the first three interfaces in the deep water model, there are many migration noises near the interfaces of the imaging result using the KBM method; this effect is seen more clearly in the partial enlarged view, while in the result of CS-KBM based results, the interfaces are clearer. For the inserted high-speed body in the right part of the model, the migration result obtained by applying the CS-KBM method also has better noise suppression. In general, the structures in the deep water model could both be distinguished in the results of the two methods; however, by employing CS-LRT to decompose the seismic records,

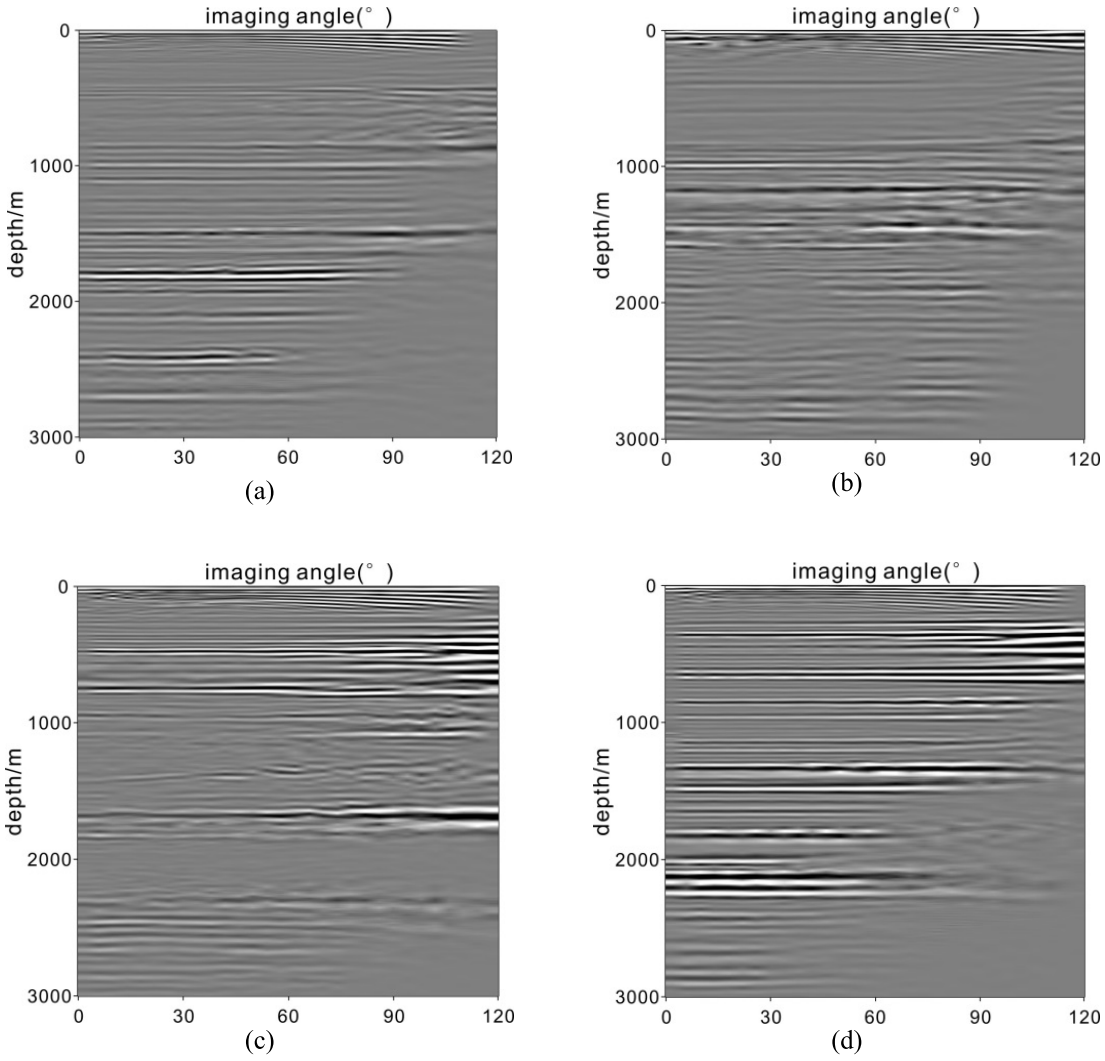

FIGURE 11. Angle gathers of CS-KBM for Marmousi model. (a) angle gather at the CDP 350; (b) angle gather at the CDP 450; (c) angle gather at the CDP 550; and (d) angle gather at the CDP 650.

CS-KBM has a better noise suppression ability and can obtain a cleaner migration section.

B. MIGRATION IMAGING OF MARMOUSI MODEL

The Marmousi model has a 737 × 750 surface area; the horizontal grid spacing is 12.5 m; the vertical grid spacing is 4.0 m. Fig. 9 shows a sample Marmousi model. The seismic data sets of the Marmousi model contain 240 shots, with 207 traces per shot, 1500 samples per trace, with a trace interval of 12.5 m and a sample rate of 2 ms. There are many steep dip interfaces, faults and folds in the Marmousi model.

Fig. 10 shows the migration results for Marmousi model using CS-KBM. In the shallow part of the model, the low-inclination interfaces on the right can be fully displayed. Though the high-inclination interfaces and faults in this step are not fully displayed, as in the low-inclination case, they are easily distinguished in the migration section. In the mid-section of the model, the faults, the high inclination interfaces and the low-inclination interfaces are all revealed clearly. In the deep section of the model, the two complex folds are easily distinguished in the migration result. CS-KBM provides a clean image of the Marmousi model in both deep and shallow structures. In summary, CS-KBM demonstrates good adaptability to the Marmousi model. Fig. 11 shows the angle gathers of the Marmousi model's migration result at the CDP 350, CDP 450, CDP 550 and CDP 650 locations. In seismic data processing, the flatter the angle gathers are, the more accurate the migration results are. Fig. 11 shows that, the angle gathers of CS-KBM for the Marmousi model are almost horizontal, which indicates the migration results of these positions coincide well with the migration model. These results also suggest that the new migration algorithm can achieve a good imaging result for the Marmousi data sets.

C. MIGRATION IMAGING OF 2D SEG/EAGE SALT MODEL

As shown in Fig. 12, the 2D SEG/EAGE salt model has a 645 × 150 surface area; the grid spacing is 24.348 m in the vertical and horizontal directions. The seismic data sets

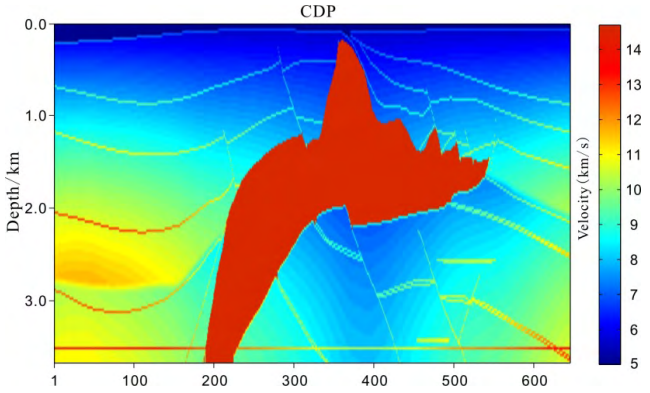

FIGURE 12. 2D SEG/EAGE salt velocity model.

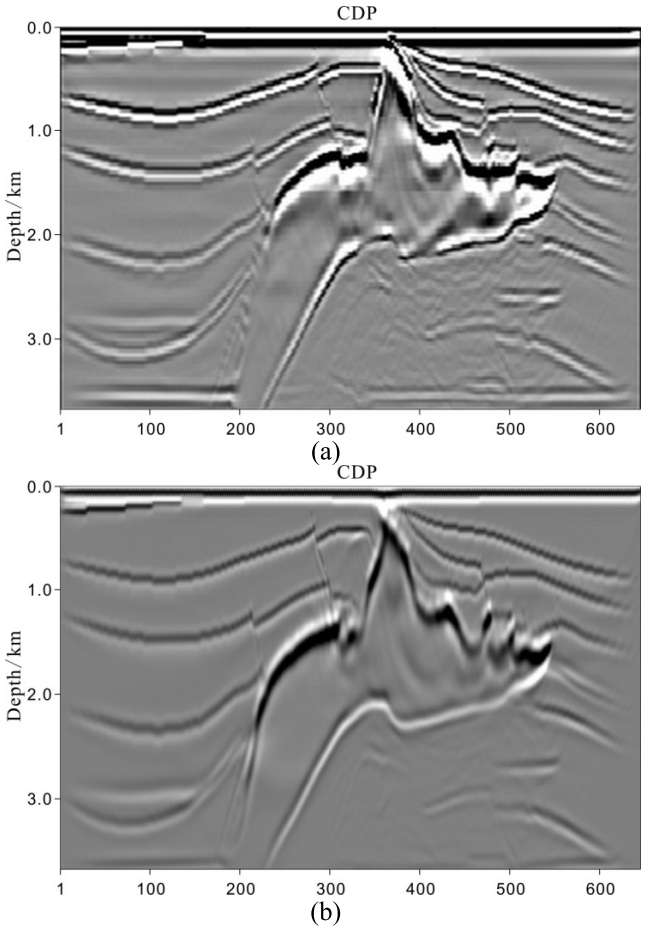

FIGURE 13. Imaging results using different migration methods on the 2D SEG/EAGE salt model. (a) result of Kirchhoff migration; (b) result of CS-KBM.

generated by the 2D SEG/EAGE salt model contain 325 shots, with 176 traces per shot, and 626 samples per trace with a sample rate of 8 ms. In addition to many interfaces and faults, the high-speed body in the model has many gear-like structures.

Fig. 13 shows the imaging results of various migration methods applied to the 2D SEG/EAGE salt model. Fig. 13 (a) shows the results for Kirchhoff migration and Fig. 13 (b) shows the result for CS-KBM. In the imaging area above the high-speed body, both migration methods can achieve a good imaging result and the interfaces and faults are displayed clearly. For imaging a high-speed body in the model, CS-KBM can clearly reveal its outline, while Kirchhoff migration could not image the steep dip interfaces and the outline in the bottom well. What's more, Kirchhoff migration produced the migration illusion for the gear-like structures on the top of the high-speed body. In the imaging area below the high-speed body, CS-KBM has a better noise suppression than Kirchhoff migration and can obtain a clearer imaging result. In general, the new method in this paper can obtain a migration section of 2D SEG/EAGE salt model with better quality.

IV. CONCLUSIONS

This paper studies the multi-arrival Kirchhoff beam migration, which focuses on obtaining high computational efficiency. To solve the low-precision and low-resolution problem of plane wave decomposition method in the prestack imaging method, CS-LRT is employed to decompose the seismic data. The improved migration algorithm was successfully applied to three complex models, including the deep water model, the Marmousi model and the 2D SEG/EAGE salt model. CS-LRT completes the task by decomposing the seismic data into plane waves from the perspective of inversion; thus, the method can achieve results of higher-resolution and better-quality results. For employing CS-LRT as its plane wave decomposition tool, the processing ability of CS-KBM is also improved.

ACKNOWLEDGMENT

The authors would like to thank Prof. Sun Jianguo, Prof. Sun Zhangqing, Prof. Han Fuxing and Prof. Gong Xiangbo in Jilin University for their kindness help.

REFERENCES

[1] X. Wang, J. Li, and Q. Chen, "Topography of the 410 km and 660 km discontinuities beneath the Japan Sea and adjacent regions by analysis of multiple-*ScS* waves," *J. Geophys. Res-Solid Earth*, vol. 122, no. 2, pp. 1264–1283, Feb. 2017.

[2] M. Dehghannejad, A. Malehmir, M. Svensson, M. Lindén, and H. Möller, "High-resolution reflection seismic imaging for the planning of a double-track tunnel in the city of Varberg, southwest Sweden," *Near Surf. Geophys.*, vol. 15, no. 3, pp. 226–240, Jun. 2017.

[3] X. Wang, K. E. Bradley, S. Wei, and W. Wu, "Active backstop faults in the Mentawai region of Sumatra, Indonesia, revealed by teleseismic broadband waveform modeling," *Earth Planetary Sci. Lett.*, vol. 483, pp. 29–38, Feb. 2018.

[4] X. Wang, S. Wei, and W. Wu, "Double-ramp on the Main Himalayan Thrust revealed by broadband waveform modeling of the 2015 Gorkha earthquake sequence," *Earth Planetary Sci. Lett.*, vol. 473, pp. 83–93, Sep. 2017.

[5] X. Wang, Q. F. Chen, J. Li, and S. Wei, "Seismic sensor misorientation measurement using P-wave particle motion: An application to the NEC-saids array," *Seismol. Res. Lett.*, vol. 87, no. 4, pp. 901–911, 2016.

[6] S.-Y. Liu, H.-Z. Wang, T.-C. Liu, Y. Hu, and C. Zhang, "Kirchhoff PSDM angle-gather generation based on the traveltime gradient," *Appl. Geophys.*, vol. 12, no. 1, pp. 83–93, Mar. 2015.

[7] H.-J. Song, J.-H. Zhang, and Z.-X. Yao, "Normal moveout for long offset in isotropic media using the Padé approximation," *Appl. Geophys.*, vol. 13, no. 4, pp. 658–666, Dec. 2016.

[8] G.-F. Liu, X.-H. Meng, and H. Liu, "Accelerating finite difference wavefield-continuation depth migration by GPU," *Appl. Geophys.*, vol. 9, no. 1, pp. 41–48, Mar. 2012.
[9] J.-J. Yang, X.-W. Luan, G. Fang, X.-X. Liu, J. Pan, and X.-J. Wang, "Elastic reverse-time migration based on amplitude-preserving P-and S-wave separation," *Appl. Geophys.*, vol. 13, no. 3, pp. 500–510, Sep. 2016.
[10] X.-D. Sun, Z.-H. Ge, Z.-C. Li, and Y. Hong, "The stability problem of reverse time migration for viscoacoustic VTI media," *Appl. Geophys.*, vol. 13, no. 4, pp. 608–613, Dec. 2016.
[11] N. R. Hill, "Gaussian beam migration," *Geophysics*, vol. 55, no. 11, pp. 1416–1428, Nov. 1990.
[12] Y. Sun, Q. Fu, S. Checkles, and J. Leveille, "3-D prestack Kirchhoff beam migration for depth imaging," *Geophysics*, vol. 65, no. 5, pp. 1592–1603, May 2000.
[13] N. Hill, "Prestack Gaussian-beam depth migration," *Geophysics*, vol. 66, no. 4, pp. 1240–1250, Apr. 2001.
[14] Z. Gao, J. Sun, H. Sun, X. Sun, P. Yu, and M. Liu, "A fast algorithm for prestack Gaussian beam migration adopting the steepest descent approximation," *Stud. Geophysica Geodaetica*, vol. 61, no. 3, pp. 575–586, Jan. 2017.
[15] R. Nowack, M. Sen, and P. Stoffa, "Gaussian beam migration for sparse common-shot and common-receiver data," in *Proc. SEG Int. Annu. Meeting*, Houston, TX, USA, 2003, pp. 1114–1117.
[16] S. Gray, "Gaussian beam migration of common-shot records," *Geophysics*, vol. 70, no. 4, pp. S71–S77, Apr. 2005.
[17] C. Gao, J. Sun, P. Qi, H. Sun, Z. Liu and M. Chen, "2D Gaussian beam migration of common shot records in time domain," *Chin. J. Geophys.-CH.*, vol. 58, no. 4, pp. 1333–1340, Apr. 2015.
[18] J. W. C. Sherwood, K. Sherwood, K. Schleicher, and H. Tieman, "3D beam prestack depth migration with examples from around the world," in *Proc. SEG Int. Annu. Meeting*, Houston, TX, USA, 2008, pp. 438–442.
[19] J. Sherwood, K. Sherwood, H. Tieman, and K. Schleicher, "3D beam prestack depth migration with examples from around the world," *Lead. Edge*, vol. 28, no. 9, pp. 1120–1127, Sep. 2009.
[20] X. Shi, S. Jian-Guo, S. Hui, L. Ming-Chen, and L. Zhi-Qiang, "The time-domain depth migration by the summation of delta packets," *Chin. J. Geophys.-Ed.*, vol. 59, no. 7, pp. 2641–2649, Jul. 2016.
[21] Y. Yue, Z.-C. Li, P. Zhang, X.-F. Zhou, and N. Qin, "Prestack Gaussian beam depth migration under complex surface conditions," *Appl. Geophys.*, vol. 7, no. 2, pp. 143–148, Jun. 2010.
[22] J. Yang, J. P. Huang, X. Wang, and Z. C. Li, "Amplitude-preserved Gaussian beam migration based on wave field approximation in effective vicinity under rugged topography condition," in *Proc. SEG Int. Annu. Meeting*, Houston, TX, USA, 2014, pp. 3852–3856.
[23] J. Yang, H. Jian-Ping, W. Xin, L. Zhen-Chun, and D. Xin-Yi, "Prestack fresnel beam migration method under complex topographic conditions," *Chin. J. Geophys.-Ed.*, vol. 58, no. 10, pp. 3758–3770, Oct. 2015.
[24] N. Bleistein and S. H. Gray, "Amplitude calculations for 3D Gaussian beam migration using complex-valued traveltimes," *Inverse Problems*, vol. 26, no. 8, p. 085017, 2010.
[25] Y. Zhang, S. Xu, N. Bleistein, and G. Zhang, "True-amplitude, angle-domain, common-image gathers from one-way wave-equation migrations," *Geophysics*, vol. 72, no. 1, pp. S49–S58, Jan. 2007.
[26] S. Gray and N. Bleistern, "True-amplitude Gaussian-beam migration," *Geophysics*, vol. 74, no. 2, pp. S11–S23, Feb. 2009.
[27] M. Popov, N. Semtchenok, and P. Popov, "Depth migration by the Gaussian beam summation method," *Geophysics*, vol. 75, no. 2, pp. S81–S93, Feb. 2010.
[28] J. Liu and G. Multiarrival, "Multiarrival Kirchhoff beam migration," *Geophysics*, vol. 76, no. 5, pp. WB109–WB118, May 2011.
[29] J. Liu and C. Marcinkovich, "Shot-profile Kirchhoff beam migration," in *Proc. SEG Annu. Meeting*, Houston, TX, USA, 2013, pp. 3969–3973.
[30] J. Han, Y. Wang, N. Han, Z.-T. Xing, and J. Lu, "Multiwave velocity analysis based on Gaussian beam prestack depth migration," *Appl. Geophys.*, vol. 11, no. 2, pp. 186–196, Jun. 2014.
[31] J. Wu, X.-H. Chen, M. Bai, and G.-C. Liu, "Attenuation compensation in multicomponent Gaussian beam prestack depth migration," *Appl. Geophys.*, vol. 12, no. 2, pp. 157–168, Jun. 2015.
[32] H. Sun *et al.*, "Research into the effects of seawater velocity variation on migration imaging in deep-water geology," *Earth. Sci. Res. J.*, vol. 20, no. 3, pp. H1–H7, Sep. 2016.
[33] H. Sun *et al.*, "Synthetic anaysis of model smoothing's influence on ray path, traveltime and migration imaging," *Appl. Ecol. Environ. Res.*, vol. 15, no. 3, pp. 443–452, Sep. 2017.
[34] X. Huang, J. Sun, and Z. Sun, "Local algorithm for computing complex travel time based on the complex eikonal equation," *Phys. Rev. E, Stat. Phys. Plasmas Fluids Relat. Interdiscip. Top.*, vol. 93, no. 4, p. 043307, 2016.
[35] H. Sun *et al.*, "Joint 3D traveltime calculation based on fast marching method and wavefront construction," *Appl. Geophys.*, vol. 14, no. 1, pp. 56–63, Mar. 2017.
[36] C. Li, J.-P. Huang, Z.-C. Li, and R.-R. Wang, "Preconditioned prestack plane-wave least squares reverse time migration with singular spectrum constraint," *Appl. Geophys.*, vol. 14, no. 1, pp. 73–86, Mar. 2017.
[37] K. Yang, J. Yang, J. Wu, C. Xing, and Y. Zhou, "Performance analysis of DF cooperative diversity system with OSTBC over spatially correlated Nakagami-*m* fading channels," *IEEE. Trans. Veh. Technol.*, vol. 63, no. 3, pp. 1270–1281, Mar. 2014.
[38] J. Du, P. Xiao, J. Wu, and Q. Chen, "Design of isotropic orthogonal transform algorithm-based multicarrier systems with blind channel estimation," *IET Commun.*, vol. 6, no. 16, pp. 2695–2704, Nov. 2012.
[39] K. Cui and X. Qin, "Virtual reality research of the dynamic characteristics of soft soil under metro vibration loads based on BP neural networks," *Neural Comput. Appl.*, vol. 29, no. 5, pp. 1233–1242, 2018.
[40] C. Hu and P. Stoffa, "Slowness-driven Gaussian-beam prestack depth migration for low-fold seismic data," *Geophysics*, vol. 74, no. 6, pp. WCA35–WCA45, Jun. 2017.
[41] J. Yang, J. Huang, X. Wang, Z. Li, and Y. Yang, "Data-driven Gaussian beam migration based on local similarity analysis," in *Proc. 77nd EAGE Conf. Expo.*, 2015.
[42] B. Wu, Z. Zhu, H. Yang, A. Osen, J. Hu, and H. Wang, "High resolution beam forming for 3D common offset Kirchhoff beam migration," in *Proc. SEG Annu. Meeting*, Houston, TX, USA, 2014, pp. 1–5.
[43] B. Wu and Z. Zhu, "Least square inversion beam forming for Kirchhoff beam migration," in *Proc. SEG Annu. Meeting*, Beijing, China, 2014, pp. 511–514.
[44] H. Wang, F. Bo, L. Shao-Yong, H. Jiang-Tao, W. Xiong-Wen, and L. Hui, "Characteristic wavefield decomposition, imaging and inversion with prestack seismic data," *Chin. J. Geophys.-Ed.*, vol. 58, no. 6, pp. 2024–2034, Jun. 2015.
[45] H. Wang, B. Feng, and X. Wang, "Compressed sensing and its application in seismic exploration," *Geophys. Prospect Petrol.*, vol. 55, no. 4, pp. 467–474, Apr. 2016.
[46] S. Liu, H. Wang, and B. Feng, "The characteristic wave decomposition and imaging in VTI media," *J. Appl. Geophys.*, vol. 115, pp. 51–58, Apr. 2015.
[47] X. Huang, H. Sun, and J. Sun, "Born modeling for heterogeneous media using the Gaussian beam summation based Green's function," *J. Appl. Geophys.*, vol. 131, pp. 191–201, Aug. 2016.
[48] V. Červený, M. Popov, and I. Pšencík, "Computation of wave fields in inhomogeneous media—Gaussian beam approach," *Geophys. J. Int.*, vol. 70, no. 1, pp. 109–128, Jan. 1982.

HUI SUN received the B.S. and Ph.D. degrees in geophysics from Jilin University, China, in 2011 and 2017, respectively. He is currently a Lecturer with the Faculty of Geosciences and Environmental Engineering, Southwest Jiaotong University. His research interests include seismic signal processing, seismic imaging methods, and forward modeling.

ZHIHOU ZHANG received the B.S. and M.S. degrees from Jilin University in 2005 and 2007, respectively, and the Ph.D. degree from Zhejiang University, China, in 2013, all in geophysics. He is currently a Lecturer with Southwest Jiaotong University, China, His research interests include signal processing in geophysics.

GUANGMIN HU received the B.S. degree from Nanjing University in 1986 and the M.S. and Ph.D. degrees from the Chengdu University of Technology in 1992 and 2000, respectively. He is currently a Professor with the University of Electronic Science and Technology of China. His research interests include network behavior, network security, network architecture, and signal processing.

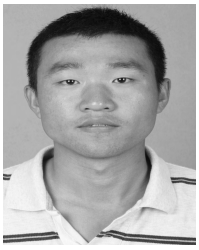

FANCHANG MENG received the B.S. and M.S. degrees in geophysics from Jilin University, China, in 2011 and 2014, respectively. He was with Chinese Railway Design Corporation from 2014 to 2017. He is currently a Doctor in seismology with the Institute of Geology and Geophysics, Chinese Academy of Science. His research interests include seismology, receiver functions, and migration images.

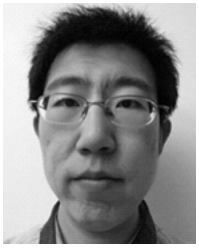

CHENG GAO received the B.S. degree in applied geophysics and the Ph.D. degree in geodetection and information technology from Jilin University, China, in 2008 and 2015, respectively. He is currently a Lecturer with the School of Mines, Inner Mongolia University of Technology, China. His research interests include seismic signal processing and migration imaging.

MINGCHEN LIU received the B.S. degree in geophysics from Jilin University, China, in 2011. He is currently a Doctor in geophysics with Jilin University. His research interests include seismology, receiver functions, and seismic migration.

JING TANG received the B.S. degree in geophysics from the Chengdu University of Technology in 2011, and the M.S. and Ph.D. degrees in geophysics from the Institute of Geology and Geophysics, Chinese Academy of Sciences, in 2014 and 2017, respectively. She is currently a Lecturer with the School of Geoscience and Technology, Southwest Petroleum University, China. Her research interests include seismic prestack inversion and stochastic inversion.

YAOJUN WANG received the B.S. degree from Anhui University in 2009 and the Ph.D. degree from the China University of Petroleum-Beijing, China, in 2015. He is currently a Lecturer with the School of Resource and Environment, University of Electronic Science and Technology of China. His research interests include seismic signal processing, seismic inversion methods, and forward modeling.

FEILONG YANG received the B.S. and M.S. degrees from Xi'an Shiyou University, China, in 2010 and 2013, respectively, and the Ph.D. degree from Chang'an University, China, in 2016, all in geophysical prospecting. He is currently a Lecturer with the School of Earth Sciences and Engineering, Xi'an Shiyou University. His research interests include seismic data processing, seismic wave field numerical modeling, and migration imaging.